Patch Antenna Sensor Rosettes for Surface Strain Measurement: Multi-physics Modeling and Experiments

Author 1

- Dan Li, PhD student
- School of Civil and Environmental Engineering, Georgia Institute of Technology, Atlanta, GA 30332, USA

Author 2

- Chunhee Cho, PhD
- School of Civil and Environmental Engineering, Georgia Institute of Technology, Atlanta, GA 30332, USA

Author 3

- Yang Wang*, Associate Professor
- School of Civil and Environmental Engineering, Georgia Institute of Technology, Atlanta, GA 30332, USA

Full contact details of corresponding author.

*yang.wang@ce.gatech.edu; phone 1 (404) 894-1851; fax 1 (404) 894-2278

Abstract

Passive (battery-free) wireless patch antenna sensors have been developed in recent years for strain sensing, to provide convenient and low-cost instrumentation. Despite past efforts, current analytical and experimental studies have mainly focused on performance in single-axial measurement, which is simple and unrealistic from typically encountered arbitrary plane stress fields. This research presents strain sensor rosettes made of folded patch antennas and slotted patch antennas for measuring an arbitrary surface strain (plane stress) field. The transverse strain effect of both sensors has been discussed and validated through laboratory experiments. Multi-physics coupled simulation is conducted to accurately describe the mechanical and electromagnetic behaviors of antenna sensors. Resonance frequency shifts of the antenna sensors are used to derive the three strain components in an arbitrary plane stress scenario, i.e. two normal and one shear strain components. Both numerical studies and experimental validations have been performed.

Keywords:

Health & Safety; Modelling; Strain

List of notation

f_0 resonance frequency of a patch antenna sensor without strain

c speed of light

$L_\mathrm{l}, L_\mathrm{t}$ length of current path of a patch antenna sensor in its longitudinal direction and transverse direction, respectively

L_total total length of current path of a patch antenna sensor

L' additional length due to fringing effect

$\beta_\mathrm{r,eff}$ effective dielectric constant of the substrate

f_ϵ resonance frequency of a patch antenna sensor under strain

Δf change of resonance frequency of a patch antenna sensor

$\widetilde{\epsilon_\mathrm{l}}, \widetilde{\epsilon_\mathrm{t}}$ strain of a patch antenna sensor in its longitudinal direction and transverse direction, respectively

$\epsilon_\mathrm{l}, \epsilon_\mathrm{t}$ strain of the base structure under a patch antenna sensor in sensor's longitudinal direction and transverse direction, respectively

η_{l}, η_{t} strain transfer ratios of a patch antenna sensor in its longitudinal direction and transverse direction, respectively

S_{l}, S_{t} strain sensitivities of a patch antenna sensor in its longitudinal direction and transverse direction, respectively

$\epsilon_{\mathrm{x}}, \epsilon_{\mathrm{y}}, \epsilon_{\mathrm{xy}}$ strain components of the base structure under Cartesian coordinates

θ_i angle between x-axis and the longitudinal direction of Sensor i in a strain sensor rosette $(i = 1, 2, 3)$

$\mathbf{T}$ transformation matrix of a strain sensor rosette

$\mathbf{S}$ strain sensitivity matrix of a strain sensor rosette

1 Introduction

Strain is one of the most important physical indicators that can quantify the performance and condition of civil structures. Traditional strain sensing systems usually utilize cable connected equipment for data acquisition, such as metal foil strain gages and fiber optic sensors. As a result, these systems suffer from high installation cost and inconvenient application when many sensors need to be installed over a large-scale structure (Spencer et al., 2004). The emergence of wireless sensors, especially recently developed passive wireless sensors which do not need battery or other onboard power supply, has shown promise to overcome the cable-related difficulties (Butler et al., 2002, Tan et al., 2008).

One example of passive wireless strain sensors is microstrip patch antenna sensor, whose resonance frequency changes when strain is applied. Tata *et al.* have investigated the potential of a rectangular microstrip patch antenna on strain sensing (Tata et al., 2009). First using cabled measurement, the linear relationship between resonance frequency of the antenna and strain is validated (Tata et al., 2009). The relationship is later verified by wireless interrogation (Deshmukh and Huang, 2010). As the rectangular microstrip patch antenna is only sensitive to strain along the longitudinal direction or the transverse direction, Daliri *et al.* propose a circular microstrip patch antenna sensor (Daliri et al., 2012) that responds to surface strain. However, the sensor cannot distinguish the three surface strain components when an arbitrary strain field is applied.

Another widely investigated approach for passive wireless sensing is radio frequency identification (RFID) technology. The RFID technology can offer the ability to modulate the response signal from the sensor (EPCglobal Inc., 2008) and thus distinguish it from environmental reflection. In recent years, many passive wireless strain sensors based on RFID technology have been proposed. A printed RFID patch antenna has been shown to measure high strain with the change of antenna gain and impedance (Merilampi et al., 2011). Meanwhile, Occhiuzzi *et al.* demonstrate the relationship between strain and electromagnetic behaviors of a meander-line RFID antenna sensor (Occhiuzzi et al., 2011). In order to reduce the size of an RFID patch antenna sensor, Yi *et al.* propose an antenna folding technique using vias, and validate the performance of the folded patch antenna sensor by tensile experiments (Yi et al., 2011). To achieve further size reduction of the RFID patch antenna sensor, slots are added on the top copper cladding to provide a detoured current path, the length of which determines antenna resonance frequency (Yi et al., 2013a, Yi et al., 2013b). Multi-

physics simulation coupling mechanics and electromagnetics is proposed to more accurately describe the behavior of the sensor (Yi et al., 2013a, Yi et al., 2013b).

Although the achievements in previous research have shown great potential in wireless strain sensing, most of the studies only address scenarios when either longitudinal or transverse strain are applied separately. Wireless strain sensing of an arbitrary surface strain field, with three strain components applied simultaneously, has not been thoroughly investigated. In this paper, strain sensor rosettes made of folded patch antenna sensors or slotted patch antenna sensors are proposed to measure an arbitrary surface strain field. The strain sensing mechanism of patch antenna sensors is studied first. In order to achieve accurate strain measurements, the transverse strain effect of patch antenna sensors is investigated through laboratory experiments and the method to consider this effect is proposed. To thoroughly investigate the strain sensing performance of both the rosettes, multi-physics simulation coupling mechanics and electromagnetics is conducted to study the electromagnetic behaviors of antenna sensors under strain. To better understand the strain sensing performance using patch antenna sensor rosettes, the consistency between one sensor scenario and a rosette scenario, as well as the effect of base structure dimensions, have been studied.

The rest of this paper is organized as follow. Section 2 introduces the rosette strain sensing mechanism of patch antenna sensors. Section 3 proposes the method to consider the transverse strain effect in the rosette setup. Section 4 presents the mechanics-electromagnetics coupled finite element models and the strain sensing simulation results. Finally, the paper is summarized with conclusion and future work.

2 Rosette strain sensing mechanism of wireless patch antenna sensors

This section provides the quantitative relationship between the resonance frequency of a patch antenna sensor and the strain experienced by the sensor. Section 2.1 introduces the strain sensing mechanism of a single patch antenna sensor. The generic formulation is applicable to both folded patch antenna sensors and slotted patch antenna sensors. Section 2.2 presents the experiment validation on the strain sensing mechanism of both types of sensors. Section 2.3 shows the strain rosette of two types of antenna sensors.

2.1 Strain sensing mechanism of a single patch antenna sensor

Figure 1(a) illustrates the design of a folded patch antenna sensor; Figure 1(b) illustrates the design of a slotted patch antenna sensor. Each figure shows the top side of the patch antenna sensors, where top

copper cladding, matching line, and RFID chip are mounted on a substrate. The bottom side of the sensor is the electronic ground plane and is also made of copper cladding. Vias through the substrate connect the top copper cladding and the electric ground in order to reduce the size of the antenna sensor. The matching line in Figure 1(a) is designed to achieve the best impedance matching between the folded patch antenna sensor and the RFID chip. The geometry pattern of the slotted patch antenna sensor is designed to have the best impedance matching between the antenna and the RFID chip, so there is no independent matching line in the slotted patch antenna sensor. In each figure, dashed arrows illustrate electrical current path on the top copper cladding of the antenna sensor. For folded patch antenna sensor, the current path is a straight line; for slotted patch antenna sensor, the current path is detoured around the slots.

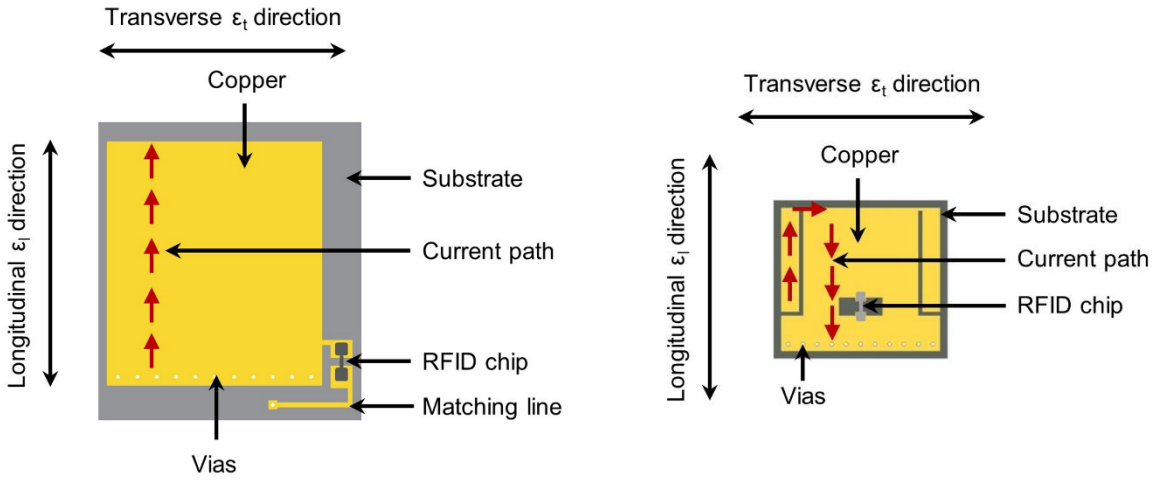

(a) Folded patch antenna (69 × 61 × 0.787 mm) (b) Slotted patch antenna (44 × 48 × 0.787 mm)

Figure 1. Illustration of patch antenna sensors

The underlying physics of a patch antenna sensor for strain sensing is that the electromagnetic resonance frequency of the patch antenna changes under strain. When strain is applied on the sensor, the length of electrical current path changes accordingly, and thus the resonance frequency changes. This change in resonance frequency of the patch antenna sensor can be wirelessly detected through RIFD technology (Yi et al., 2011). An RFID reader emits a wireless interrogation signal to the sensor, which in turn harness energy from the signal for its own operation. When the interrogation frequency equals to the resonance frequency of the patch antenna sensor, best matching between antenna and the RFID chip occurs, and thus least interrogation power is needed to activate the RFID chip. By recording the interrogation frequency corresponding to the minimum value of interrogation power, the resonance frequency of the patch antenna is obtained and then used to derive the amount of strain. In general, Eq. (1) shows the relationship between

77 the resonance frequency and the geometric property of a patch antenna that has the row of vias connecting
78 top copper cladding to the ground plane:

$$f_0 = \frac{c}{2(L_\mathrm{l} + L_\mathrm{t} + L')\sqrt{\beta_{\mathrm{r,eff}}}} = \frac{c}{2L_{\mathrm{total}}\sqrt{\beta_{\mathrm{r,eff}}}} \quad (1)$$

79 where c is the speed of light; L_l is the length of current path in longitudinal direction; L_t is the length of
80 current path in transverse direction; L' is the additional length due to fringing effect; L_{total} is the total length
81 of current path; $\beta_{\mathrm{r,eff}}$ is the effective dielectric constant. Figure 1 illustrates the longitudinal and transverse
82 directions of each sensor. As shown in the Figure 1, a folded patch antenna sensor does not have
83 transverse current path but a slotted patch antenna sensor has transverse current path. For simplicity, past
84 studies of slotted patch antenna strain sensors usually consider L_t to be much smaller than L_l, and thus do
85 not include the current path in transverse direction (Yi et al., 2013b, Yi et al., 2014). However, in order to
86 obtain an accurate strain measurement, this study will demonstrate that the transverse strain effect should
87 be considered, particularly for slotted antenna sensors.
88 When the patch antenna is under relatively small longitudinal strain $\widetilde{\epsilon_\mathrm{l}}$ and transverse strain $\widetilde{\epsilon_\mathrm{t}}$, the
89 resonance frequency of the antenna changes to:

$$\begin{aligned} f_\epsilon &= \frac{c}{2(L_\mathrm{l}(1+\widetilde{\epsilon_\mathrm{l}}) + L_\mathrm{t}(1+\widetilde{\epsilon_\mathrm{t}}) + L')\sqrt{\beta_{\mathrm{r,eff}}}} \\ &= \frac{f_0}{1 + \frac{L_\mathrm{l}}{L_{\mathrm{total}}}\widetilde{\epsilon_\mathrm{l}} + \frac{L_\mathrm{t}}{L_{\mathrm{total}}}\widetilde{\epsilon_\mathrm{t}}} \\ &\approx f_0\left(1 - \frac{L_\mathrm{l}}{L_{\mathrm{total}}}\widetilde{\epsilon_\mathrm{l}} - \frac{L_\mathrm{t}}{L_{\mathrm{total}}}\widetilde{\epsilon_\mathrm{t}}\right) \end{aligned} \quad (2)$$

90 The equation shows that the resonance frequency is approximately linear to the strain on the antenna
91 sensor, in particular if the strain is small. Due to the bonding effect between the antenna sensor and the
92 base structure, only some percentage of the strain in the base structure can be transferred to the antenna
93 sensor. Longitudinal strain transfer ratio η_l refers to the percentage of the longitudinal strain on the sensor
94 $\widetilde{\epsilon_\mathrm{l}}$ over the longitudinal strain on the base structure ϵ_l; transverse strain transfer ratio η_t refers to the
95 percentage of the transverse strain on the sensor $\widetilde{\epsilon_\mathrm{t}}$ over the transverse strain on the base structure ϵ_t.
96 Both ratios are close to but less than 100%. We use Δf to denote the change of the resonance frequency

of the antenna sensor when strain ϵ_{l} and ϵ_{t} occur on the surface of the base structure. Based on the linear relationship shown in Eq. (2), the relationship between Δf and ϵ_{l}, ϵ_{t} is obtained as:

$$\Delta f = f_{\epsilon} - f_0 \approx -\frac{f_0 L_{\mathrm{l}}}{L_{\mathrm{total}}}\widetilde{\epsilon_{\mathrm{l}}} - \frac{f_0 L_{\mathrm{t}}}{L_{\mathrm{total}}}\widetilde{\epsilon_{\mathrm{t}}} = -\frac{f_0 L_{\mathrm{l}}}{L_{\mathrm{total}}}\eta_{\mathrm{l}}\epsilon_{\mathrm{l}} - \frac{f_0 L_{\mathrm{t}}}{L_{\mathrm{total}}}\eta_{\mathrm{t}}\epsilon_{\mathrm{t}} = S_{\mathrm{l}}\epsilon_{\mathrm{l}} + S_{\mathrm{t}}\epsilon_{\mathrm{t}} \quad (3)$$

where S_{l} is named the longitudinal strain sensitivity and S_{t} is named the transverse strain sensitivity. Each sensitivity number represents the linear proportional relationship between resonance frequency and the strain along that direction.

2.2 Experiment validation

To better illustrate the transverse strain sensitivity of a patch antenna sensor, tensile tests on folded patch antenna sensors and slotted patch antenna sensors have been conducted. Figure 2(a) shows the center region of an aluminum specimen with two folded patch antenna sensors installed in perpendicular orientations. Sensor 1 has its longitudinal direction oriented along the y-axis (loading direction), while Sensor 2 has its longitudinal direction along the x-axis. Likewise, Figure 2(b) shows the center region of an aluminum specimen with two slotted patch antenna sensors installed. Similarly, Sensor 1 has its longitudinal direction oriented along the y-axis (loading direction), while Sensor 2 has its longitudinal direction along the x-axis. Each specimen is 610 mm long, 150 mm wide, and 3.2 mm thick. For each specimen, loading direction is along y-axis; the specimen deforms freely along the lateral x direction. Ten reference metal foil strain gages are installed on each specimen, five measuring ϵ_{y} and five measuring ϵ_{x}.

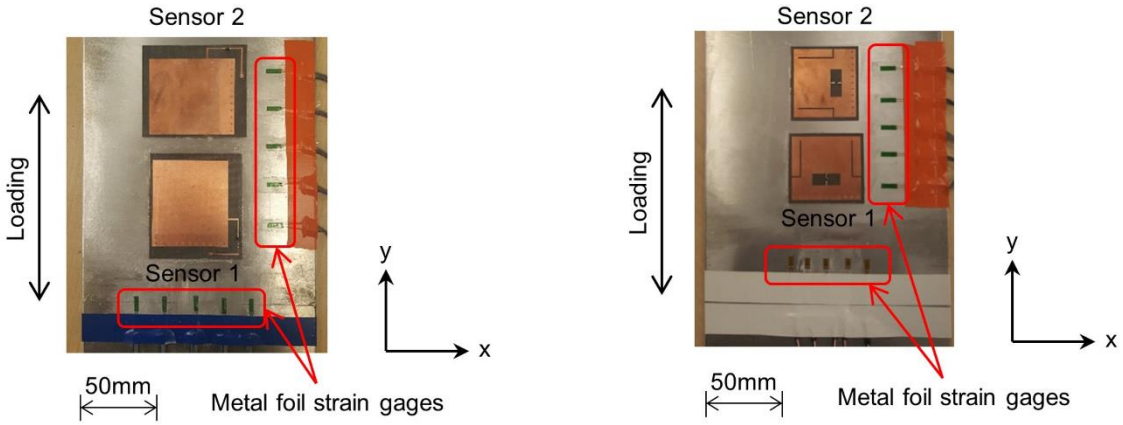

(a) Folded patch antennas (b) Slotted patch antennas

Figure 2. Sensor instrumentation for tensile test

As shown in Eq. (3), strain sensitivities are mainly determined by the lengths of electric current paths. Because the actual current paths on a fabricated sensor are determined by the sensor geometry, it is

preferable that the sensor fabrication is as accurate as possible. Another important factor on strain sensitivity is strain transfer ratio. To achieve a high strain transfer ratio, strong bonding is needed when installing the antenna sensors. Other factors, such as interrogation distance, specimen size, and loading method, are found to have smaller effect on the strain sensitivity of antenna sensors.

The axial force applied by the tensile machine is configured so that approximately a +50 με along y-axis is achieved at each loading step. Meanwhile, the specimen shrinks along x-axis due to Poisson's effect. The test starts with $\epsilon_y = 0$ με, and ends at around $\epsilon_y = 350$ με. At each loading step, the resonance frequencies for both sensors and the strain for both directions are recorded.

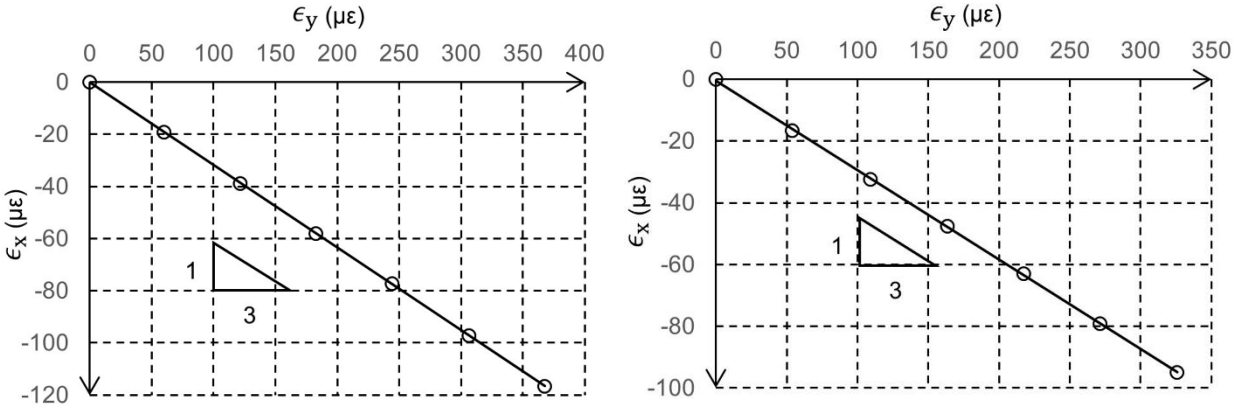

(a) Seven loading steps for specimen with folded patch antenna sensors

(b) Seven loading steps for specimen with slotted patch antenna sensors

Figure 3. Strain ϵ_y versus ϵ_x measured by metal foil strain gages

Table 1. Resonance frequencies of patch antenna sensors (MHz)

Loading step	Folded patch antenna sensor		Slotted patch antenna sensor	
	Sensor 1	Sensor 2	Sensor 1	Sensor 2
1	909.663	904.027	912.445	912.836
2	909.618	904.041	912.422	912.832
3	909.570	904.051	912.366	912.825
4	909.533	904.076	912.320	912.817
5	909.494	904.084	912.271	912.821
6	909.460	904.091	912.234	912.815
7	909.382	904.114	912.199	912.795

For each specimen, Figure 3 shows the strain ϵ_y versus ϵ_x measured by metal foil strain gages. The slope of each plot is around 1/3 which is close to the Poisson's ratio of aluminum. Table 1 lists the resonance frequencies of patch antenna sensors at all loading steps. Using the strain and resonance frequency data,

the longitudinal and transverse strain sensitivities of each sensor can be calculated through linear regression according to Eq. (3). This leads to a least squares problem with longitudinal and transverse strain sensitivities, S_{l} and S_{t}, as optimization variables:

$$\underset{S_{\mathrm{l}},S_{\mathrm{t}}}{\text{minimize}} \sum_{i} [\Delta f_i - (S_{\mathrm{l}}\epsilon_{\mathrm{l}i} + S_{\mathrm{t}}\epsilon_{\mathrm{t}i})]^2 \tag{4}$$

Upon solving the least squares problem using available data points, Table 2 lists the longitudinal and transverse strain sensitivities of both sensors. The folded patch antenna sensor has a transverse strain sensitivity of 25 Hz/με, which is close to 0 Hz/με. This is because transverse strain cannot significantly change the total length of current path for a folded patch antenna sensor. On the other hand, due to the complicated geometry of a slotted patch antenna sensor, transverse strain changes the total length of current path of the sensor. Thus, the slotted patch antenna sensor has a relatively high transverse strain sensitivity, which is around -362.3 Hz/με.

Table 2. Strain sensitivities for patch antenna sensors (Hz/με)

Folded patch antenna sensor		Slotted patch antenna sensor	
Longitudinal S_{l}	Transverse S_{t}	Longitudinal S_{l}	Transverse S_{t}
-801.2	25.3	-794.6	-362.3

2.3 Strain rosettes of antenna sensors

Most studies of patch antenna strain sensors have been limited to uniaxial measurement (Yi et al., 2011, Yi et al., 2014). In order to measure an arbitrary surface strain field, strain rosettes (Boresi and Schmidt, 2002) made of folded patch antennas or slotted patch antennas need to be deployed. Figure 4 (a) and Figure 4 (b) show the rosette schematic for each sensor type, respectively. Each rosette consists of three patch antenna sensors, with the three sensors rotated at 120º intervals. In each rosette, the longitudinal axis of Sensor 1 is placed along y-axis, Sensor 2 is rotated 120º counterclockwise from y-axis, and Sensor 3 is rotated 120º clockwise from y-axis. Because off-the-shelf RFID modulation technology mostly operates at around 900MHz, the dimension the antenna sensors and thus, of the rosette is larger than a typical metal foil strain rosette. It is preferable to have a fairly uniform strain field under the rosette area, or the measurement result will be the average strain.

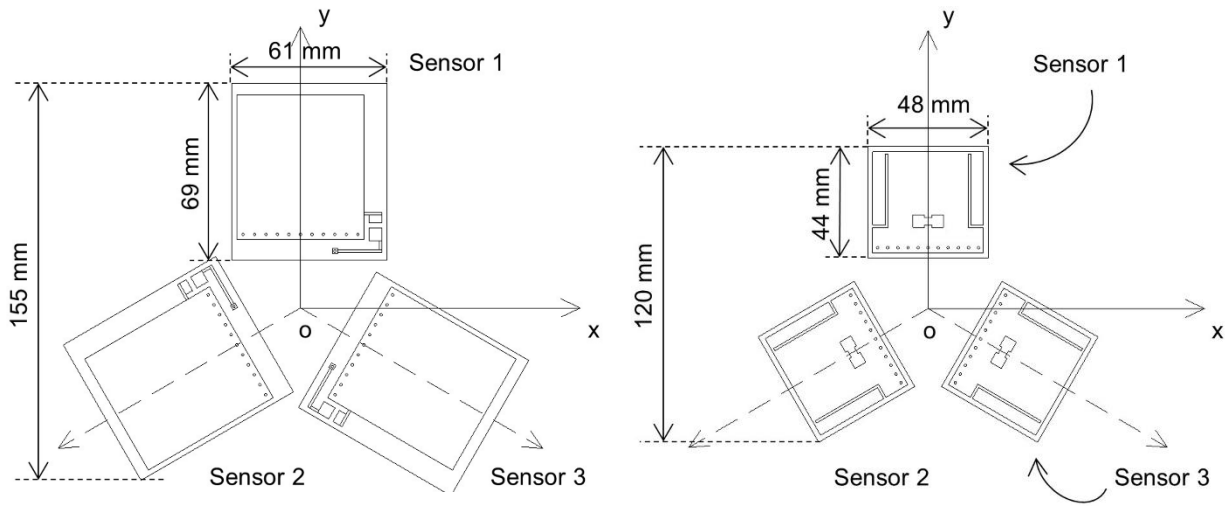

(a) Rosette with three folded patch antennas (b) Rosette with three slotted patch antennas

Figure 4. Schematic of the two types of strain rosettes

Consider each rosette is mounted on a flat surface area for strain measurement, the three strain components under Cartesian coordinates are denoted as ϵ_{x}, ϵ_{y}, and ϵ_{xy}. They are related to the longitudinal strains of base structure under the three sensors, $\epsilon_{\mathrm{l},1}$, $\epsilon_{\mathrm{l},2}$, and $\epsilon_{\mathrm{l},3}$ by the strain transformation equations:

$$\begin{Bmatrix}\epsilon_{\mathrm{l},1}\\ \epsilon_{\mathrm{l},2}\\ \epsilon_{\mathrm{l},3}\end{Bmatrix}=\begin{bmatrix}\frac{1+\cos(2\theta_1)}{2} & \frac{1-\cos(2\theta_1)}{2} & \sin(2\theta_1)\\ \frac{1+\cos(2\theta_2)}{2} & \frac{1-\cos(2\theta_2)}{2} & \sin(2\theta_2)\\ \frac{1+\cos(2\theta_3)}{2} & \frac{1-\cos(2\theta_3)}{2} & \sin(2\theta_3)\end{bmatrix}\begin{Bmatrix}\epsilon_{\mathrm{x}}\\ \epsilon_{\mathrm{y}}\\ \epsilon_{\mathrm{xy}}\end{Bmatrix} \tag{5}$$

where θ_1 is the angle between x-axis and the longitudinal direction of Sensor 1, which equals to 90º; θ_2 is the angle between x-axis and the longitudinal direction of Sensor 2, which equals to 210º; θ_3 is the angle between x-axis and the longitudinal direction of Sensor 3, which equals to 330º. Therefore, in each rosette, from the longitudinal strains measured by three sensors, the three strain components can be calculated as:

$$\begin{Bmatrix}\epsilon_{\mathrm{x}}\\ \epsilon_{\mathrm{y}}\\ \epsilon_{\mathrm{xy}}\end{Bmatrix}=\frac{1}{3}\begin{bmatrix}-1 & 2 & 2\\ 3 & 0 & 0\\ 0 & \sqrt{3} & -\sqrt{3}\end{bmatrix}\begin{Bmatrix}\epsilon_{\mathrm{l},1}\\ \epsilon_{\mathrm{l},2}\\ \epsilon_{\mathrm{l},3}\end{Bmatrix}=\mathbf{T}\begin{Bmatrix}\epsilon_{\mathrm{l},1}\\ \epsilon_{\mathrm{l},2}\\ \epsilon_{\mathrm{l},3}\end{Bmatrix} \tag{6}$$

where $\mathbf{T}$ is the transformation matrix which maps the longitudinal strains measured three sensors onto the three strain components under Cartesian coordinates.

3 Consideration of transverse strain effect

When measuring a surface strain field by the strain sensor rosette, the transverse strain sensitivity of each antenna sensor should be considered. Transverse strain sensitivity in a patch antenna sensor refers to the

change of resonance frequency due to strain in the transverse direction of the sensor. The transverse strain effect should be considered in order to obtain the accurate longitudinal strain value.

For an antenna sensor exposed to an arbitrary surface strain field, the change of the resonance frequency may contain contribution from both longitudinal and transverse strains. Eq. (3) is repeated for convenience:

$$\Delta f = S_{\mathrm{l}}\epsilon_{\mathrm{l}} + S_{\mathrm{t}}\epsilon_{\mathrm{t}} \tag{7}$$

Here ϵ_{l} is the normal strain along the longitudinal direction under the antenna sensor, ϵ_{t} is the normal strain along the transverse direction under the antenna sensor, S_{l} is the longitudinal strain sensitivity, and S_{t} is the transverse strain sensitivity. It is should be noted that S_{l} and S_{t} are defined in a uniaxial strain setting rather than a uniaxial stress setting. In accordance with practical application, it is assumed that three antenna sensors in the strain rosette share the same longitudinal strain sensitivity S_{l} and transverse strain sensitivity S_{t}. Using Eq. (6) and Eq. (7), the change of the resonance frequency of Sensor 1 in the rosette setup can be expressed as:

$$\begin{aligned}\Delta f_1 &= S_{\mathrm{l}}\epsilon_{\mathrm{y}} + S_{\mathrm{t}}\epsilon_{\mathrm{x}} \\ &= S_{\mathrm{l}}\epsilon_{\mathrm{l},1} + S_{\mathrm{t}}\left(\frac{2}{3}\epsilon_{\mathrm{l},2} + \frac{2}{3}\epsilon_{\mathrm{l},3} - \frac{1}{3}\epsilon_{\mathrm{l},1}\right) \\ &= \left(S_{\mathrm{l}} - \frac{1}{3}S_{\mathrm{t}}\right)\epsilon_{\mathrm{l},1} + \frac{2}{3}S_{\mathrm{t}}\epsilon_{\mathrm{l},2} + \frac{2}{3}S_{\mathrm{t}}\epsilon_{\mathrm{l},3}\end{aligned} \tag{8}$$

Likewise, the equations for Δf_2 and Δf_3 can be derived. The change of the resonance frequencies in all three antenna sensors can be expressed as:

$$\begin{Bmatrix}\Delta f_1 \\ \Delta f_2 \\ \Delta f_3\end{Bmatrix} = \frac{1}{3}\begin{bmatrix}3S_{\mathrm{l}} - S_{\mathrm{t}} & 2S_{\mathrm{t}} & 2S_{\mathrm{t}} \\ 2S_{\mathrm{t}} & 3S_{\mathrm{l}} - S_{\mathrm{t}} & 2S_{\mathrm{t}} \\ 2S_{\mathrm{t}} & 2S_{\mathrm{t}} & 3S_{\mathrm{l}} - S_{\mathrm{t}}\end{bmatrix}\begin{Bmatrix}\epsilon_{\mathrm{l},1} \\ \epsilon_{\mathrm{l},2} \\ \epsilon_{\mathrm{l},3}\end{Bmatrix} \tag{9}$$

where $\epsilon_{\mathrm{l},i}$ is the longitudinal strain of the i^{th} sensor. According to Eq. (6) and Eq. (9), the strain components under Cartesian coordinates can be calculated from the three frequency changes as:

$$\boldsymbol{\epsilon} = \mathbf{T}\mathbf{S}^{-1}\boldsymbol{\Delta}\mathbf{f} \tag{10}$$

where $\boldsymbol{\epsilon} = [\epsilon_x \quad \epsilon_y \quad \epsilon_{xy}]^{\mathrm{T}}$ is the strain vector, $\boldsymbol{\Delta}\mathbf{f} = [\Delta f_1 \quad \Delta f_2 \quad \Delta f_3]^{\mathrm{T}}$ is the resonance frequency change vector, and $\mathbf{S}$ is the strain sensitivity matrix for Eq. (9):

$$\mathbf{S} = \frac{1}{3}\begin{bmatrix} 3S_{\mathrm{l}} - S_{\mathrm{t}} & 2S_{\mathrm{t}} & 2S_{\mathrm{t}} \\ 2S_{\mathrm{t}} & 3S_{\mathrm{l}} - S_{\mathrm{t}} & 2S_{\mathrm{t}} \\ 2S_{\mathrm{t}} & 2S_{\mathrm{t}} & 3S_{\mathrm{l}} - S_{\mathrm{t}} \end{bmatrix} \tag{11}$$

This method to consider transverse strain effect is further studied for both types of rosettes in the next section.

4 Mechanical-electromagnetic coupled simulation

Behavior of both types of the rosettes, under arbitrary surface strain field, is first studied in numerical simulation. Section 4.1 introduces the numerical model which simulates the behavior of each rosette. Section 4.2 presents the strain sensitivities of antenna sensors in both types of rosettes. Section 4.3 shows the strain sensing performance of both rosettes under an arbitrary surface strain field.

4.1 Model details

The strain sensor rosette is modeled by ANSYS software package. Using the slotted patch antenna sensor rosette as an example, Figure 5 shows the finite element model built in ANSYS. To achieve an ideally uniform strain distribution around the rosette, an aluminum plate (500 mm × 500 mm × 25.4 mm) is used as the base structure. Along the perimeter of the plate, stiffened outlines are assigned to help generate a uniform surface strain field on the plate. Without the stiffened outlines, the edges of the aluminum plate cannot remain straight when load is applied, and thus the strain field in the rosette region may be far away from uniform. The strain rosette is placed at the center of the aluminum plate. Mechanical model of each antenna sensor consists of a top copper cladding, a substrate, and a bottom copper cladding. Partially air-filled cavity models are used to improve simulation efficiency (Carver and Mink, 1981, Daly, 1971, Cho et al., to be published). The height of the air domain is ten times the height of the substrate. Material properties used in the simulation are listed in Table 3. The stiffened outline is assigned a Young's modulus much higher than the aluminum's.

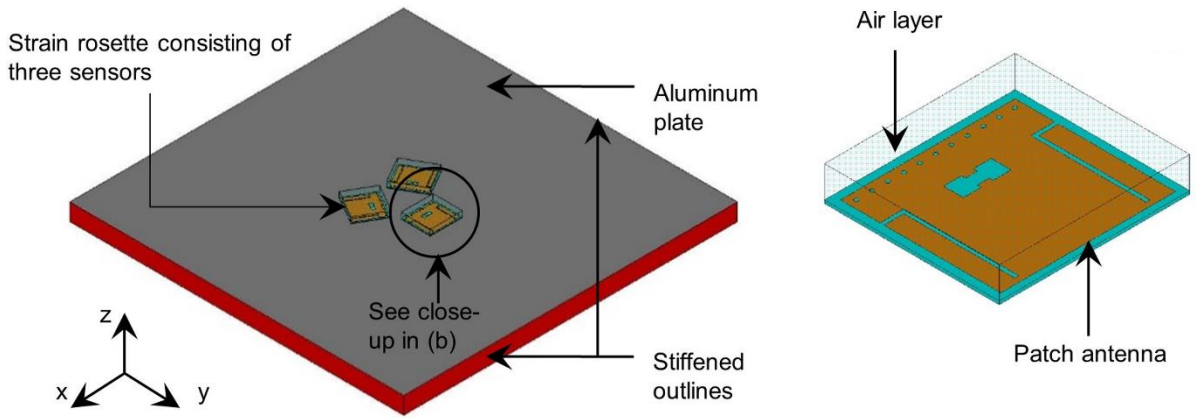

(a) The entire model

(b) Close-up view of a slotted patch antenna sensor

Figure 5. Multi-physics simulation model of an antenna sensor rosette on an aluminum plate

Table 3. Properties of material used in ANSYS simulation

	Aluminum plate	Stiffened outline	Substrate	Copper cladding	Air
Material type	6061 Aluminum alloy	–	Rogers RT/duroid® 5880	Copper	Air
Relative permittivity (β_r)	–	1	2.2	–	1
Poisson's Ratio	0.33	0.33	0.4	0.35	0
Young's modulus (GPa)	69	10000	1.07	117	0

As the electromagnetic field has little effect on mechanical field, a sequential coupled simulation approach is adopted. First, the mechanical simulation is conducted to obtain the deformed antenna shapes. Second, the electromagnetic behaviors of the antenna sensors are simulated based on the deformed shapes, so that antenna resonance frequency under strain can be identified. The mechanics-electromagnetics coupled simulation therefore accurately characterizes electromagnetic behavior of the antennas under strain.

In the mechanical simulation, the aluminum plate and the substrate of antenna sensors are simulated by tetrahedral solid elements SOLID186, while the stiffened outlines of the aluminum plate and the copper cladding of antenna sensors are simulated by shell elements SHELL181. The bonding effect between antenna sensors and the aluminum plate is treated as ideal, i.e. the bottom surface of antenna sensors and the top surface of the aluminum plate share the same nodes.

In the electromagnetic simulation, the aluminum plate and the stiffened outlines are removed while the copper cladding, the substrate of each antenna sensor, and the air layer constitute a resonance cavity. The elements of the substrate and the air are converted to high-frequency electromagnetic elements HF119.

The copper claddings are treated as perfect electric conductor (PEC), and function as boundary conditions of the cavity model. The resonance frequency of each antenna sensor is calculated by solving the generalized eigenvalue problem of the cavity model (Jin and Volakis, 1991).

4.2 Strain sensitivities for RFID antenna sensor rosette

Before validating the strain sensing performance of the strain rosette, strain sensitivities S_l and S_t of antenna sensors need to be determined. Without losing generality, Sensor 1 is taken as example to show the procedure of obtaining the strain sensitivity values. In the mechanical simulation, vertical displacements are applied on the horizontal stiffened outlines of the aluminum plate to generate normal strain $\epsilon_{l,1}$ (i.e. ϵ_y along y-axis) in the longitudinal direction of Sensor 1. Meanwhile, the other two outlines are constrained so that transverse strain $\epsilon_{t,1}$ (i.e. ϵ_x along x-axis) of Sensor 1 remains zero. Figure 6 shows the displacements assigned to the stiffened outlines to generate this uniaxial strain field for Sensor 1.

The displacements are adjusted to generate different strain levels of $\epsilon_{l,1}$ (from 0 to 2,000 με with increments of 500 με) in the aluminum plate. Figure 7 shows the strain distribution ϵ_y of the two types of rosettes when 2,000 με is applied. The figure shows that approximately uniform strain distribution ϵ_y is achieved around the center area of Sensor 1 and the strain distribution highly depends on the geometry pattern.

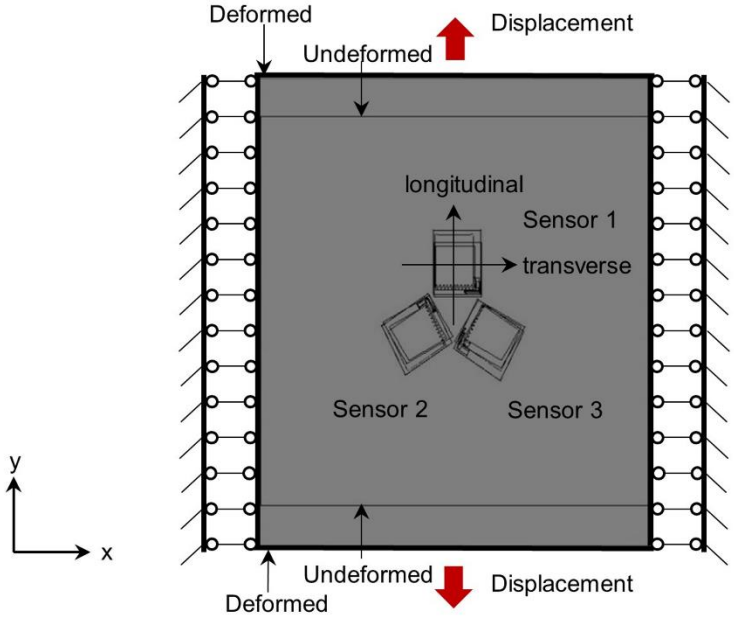

Figure 6. Displacements assigned to the stiffened outlines to generate uniaxial longitudinal strain in the Sensor 1

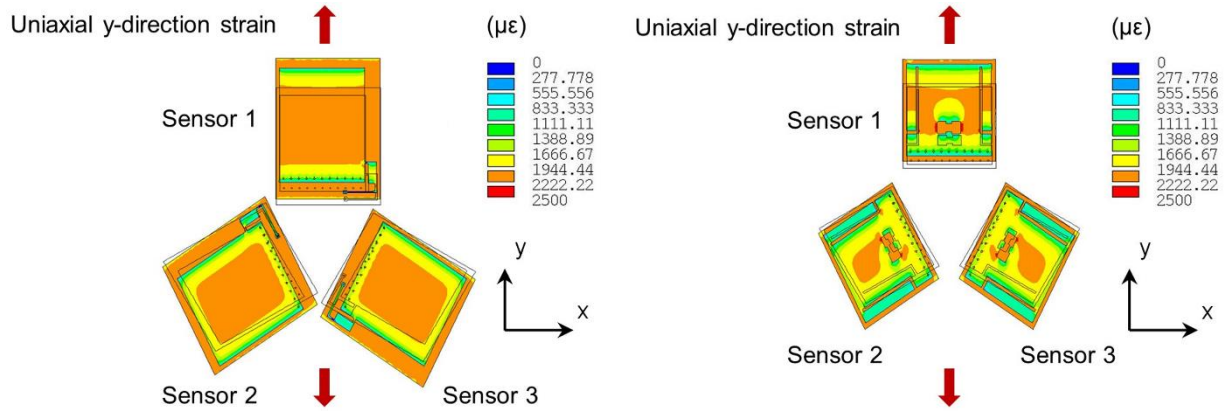

(a) Rosette with three folded patch antennas (b) Rosette with three slotted patch antennas

Figure 7. Strain distribution ϵ_y of the rosettes (when uniaxial $\epsilon_y = 2{,}000\ \mu\varepsilon$ is applied to the aluminum plate)

After simulating each strain level, resonance frequency of Sensor 1 is identified by the electromagnetic eigenfrequency solver with the deformed finite element model. Based on the strain level and corresponding resonance frequency, the strain sensitivity can be calculated. Figure 8 shows the simulated resonance frequencies at different longitudinal strains for Sensor 1 in the folded patch antenna rosette. The resonance frequency of the antenna sensor reduces from 918.409 MHz to 916.705 MHz as strain increases from 0 to 2,000 με. From the linear regression applied on the five data points, the longitudinal strain sensitivity of the antenna sensor is -851.630 Hz/με, which is shown as the slope of the curve in the figure. A similar procedure with $\epsilon_y = 0$ and ϵ_x increasing to 2,000 με is used to find the transverse strain sensitivity S_t of Sensor 1. As expected, the sensitivity turns out to be zero. For the other two folded patch sensors, because the longitudinal direction of Sensor 2 or Sensor 3 is not along x or y axis, a special strain field needs to be designed to generate uniaxial strain along the longitudinal direction of each sensor. The applied strain fields are summarized in Table 4. Displacements of the stiffened outlines are configured to generate a desired uniaxial strain field on each sensor. For example, when $\epsilon_x = 3\varepsilon/4$, $\epsilon_y = \varepsilon/4$, and $\epsilon_{xy} = \sqrt{3}\varepsilon/4$, the strain along the longitudinal direction of Sensor 2 can be calculated as $\epsilon_{l,2} = \varepsilon$ according to Eq. (5), and meanwhile the transverse strain $\epsilon_{t,2} = 0$.

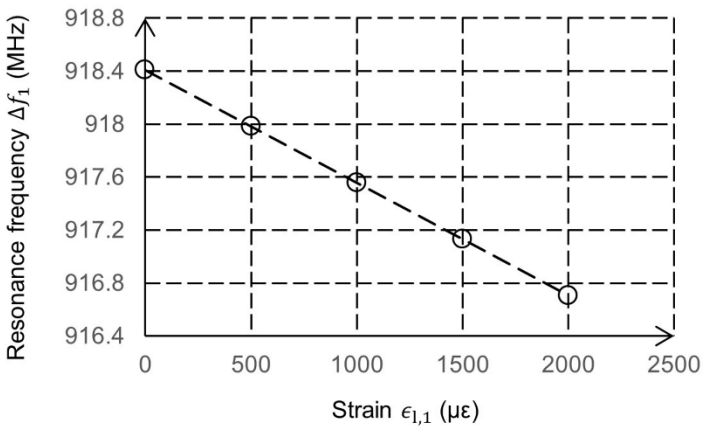

Figure 8. Longitudinal strain sensitivity of Sensor 1 in the folded patch antenna rosette ($S_{l,1} = -851.630\ \mathrm{Hz/\mu\varepsilon}$)

Table 4. Strain field applied to generate uniaxial longitudinal or uniaxial transverse strain in Sensor 2 and Sensor 3

Sensor	Desired uniaxial normal strain in the sensor	Strain field applied to the aluminum plate		
		ϵ_x	ϵ_y	ϵ_{xy}
Sensor 2	ε along the longitudinal direction $\epsilon_{l,2}$	$3\varepsilon/4$	$\varepsilon/4$	$\sqrt{3}\varepsilon/4$
	ε along the transverse direction $\epsilon_{t,2}$	$\varepsilon/4$	$3\varepsilon/4$	$-\sqrt{3}\varepsilon/4$
Sensor 3	ε along the longitudinal direction $\epsilon_{l,3}$	$3\varepsilon/4$	$\varepsilon/4$	$-\sqrt{3}\varepsilon/4$
	ε along the transverse direction $\epsilon_{t,2}$	$\varepsilon/4$	$3\varepsilon/4$	$\sqrt{3}\varepsilon/4$

In total, six loading scenarios are simulated for the plate with folded patch antenna sensor rosette, in order to identify $S_{l,1}$, $S_{t,1}$, $S_{l,2}$, $S_{t,2}$, $S_{l,3}$, and $S_{t,3}$. Likewise, six loading scenarios are simulated for the plate with slotted patch antenna sensor rosette, to identify the longitudinal and transverse strain sensitivities for each of the three sensors. Table 5 lists the simulation results of all the three sensors for both types of strain rosettes. As the meshing on three antenna sensors cannot be perfectly the same, the initial frequencies and strain sensitivities of the three sensors are very close but have slight differences. The results show that the longitudinal strain sensitivities of folded patch antenna sensors are higher than those of slotted patch antenna sensors. In addition, the transverse strain sensitivity of the folded patch antenna is zero, which makes its application straightforward when transverse strain effect exists. However, as the folded patch antenna sensor rosette does not have reflection symmetry like the slotted patch antenna sensor rosette,

the differences on initial frequencies and strain sensitivities among the three folded patch antennas are slightly larger than those among the three slotted patch antenna sensors.

Table 5. Initial resonance frequencies and strain sensitivities of three sensors in each rosette

Sensor	Folded patch antenna sensor rosette			Slotted patch antenna sensor rosette		
	Initial resonance frequency (MHz)	Strain sensitivity (Hz/με)		Initial resonance frequency (MHz)	Strain sensitivity (Hz/με)	
Sensor 1	918.409	Longitudinal $S_{l,1}$	-851.630	912.301	Longitudinal $S_{l,1}$	-771.214
		Transverse $S_{t,1}$	0		Transverse $S_{t,1}$	-220.261
Sensor 2	918.319	Longitudinal $S_{l,2}$	-854.722	912.211	Longitudinal $S_{l,2}$	-771.119
		Transverse $S_{t,2}$	0		Transverse $S_{t,2}$	-220.241
Sensor 3	918.291	Longitudinal $S_{l,3}$	-861.220	912.348	Longitudinal $S_{l,3}$	-771.031
		Transverse $S_{t,3}$	0		Transverse $S_{t,3}$	-219.655

4.3 Rosette performance in an arbitrary surface strain field

To further validate the strain sensing performance of each rosette, an arbitrary surface strain field with $\epsilon_x = -400$ με in the x direction, $\epsilon_y = 600$ με in the y direction and $\epsilon_{xy} = 200$ με shear strain is applied on the aluminum plate. Again, displacements are applied at the stiffened outlines of the aluminum plate to generate the desired strain field. Figure 9 shows the deformation of the aluminum plate with the rosettes. The thin square outline refers to the original shape of the aluminum plate and the grey area with thick outlines shows the deformed aluminum plate. Using deformed antenna shapes, the electromagnetic eigenfrequency solver computes the resonance frequencies under strain as 917.890 MHz for Sensor 1, 918.310 MHz for Sensor 2, and 918.566 MHz for Sensor 3 in folded patch antenna rosette. Based on initial resonance frequency in Table 5, the frequency change vector is calculated as $\Delta f = \{-0.519\ \text{MHz} \quad -0.009\ \text{MHz} \quad 0.275\ \text{MHz}\}^T$. From another simulation with a slotted patch antenna rosette, the results are 911.926 MHz for Sensor 1, 912.152 MHz for Sensor 2, and 912.488 MHz for Sensor 3. Similarly, the frequency change vector is calculated as $\Delta f = \{-0.375\ \text{MHz} \quad -0.059\ \text{MHz} \quad 0.140\ \text{MHz}\}^T$. Since the simulated strain sensitivities for the three antenna sensors in the rosette setup are different (see Table 5), the average of the strain sensitivities are adopted for strain measurement. For the folded patch antenna sensors, the average longitudinal strain sensitivity $S_l = -855.857$ Hz/με and the average transverse strain sensitivity $S_t = 0$ Hz/με; for the slotted patch antenna sensors, the average longitudinal strain sensitivity $S_l = -771.121$ Hz/με and the average transverse strain sensitivity $S_t = -220.052$ Hz/με. Based on the strain-induced resonance

frequency change vectors above, the three strain components ϵ_x, ϵ_y, and ϵ_{xy} under each rosette are calculated according to Eq. (10).

Table 6 shows the strain components calculated from the frequency shifts of each strain rosette. The simulation results indicate that both types of strain sensor rosettes can be used to measure the arbitrary surface strain field with acceptable errors. Because the folded patch antennas have zero transverse strain sensitivity, it is not needed to consider transverse strain effect on the resonance frequency shift. For the slotted patch antenna rosette, if the transverse strain effect is not considered, the errors increase dramatically to 41.97% for ϵ_x, 18.95% for ϵ_y, and 25.50% for ϵ_{xy}. This means for the slotted patch antennas, the transverse strain sensitivity has a significant effect on the measurement. The effects needs to be considered to obtain accurate strain components.

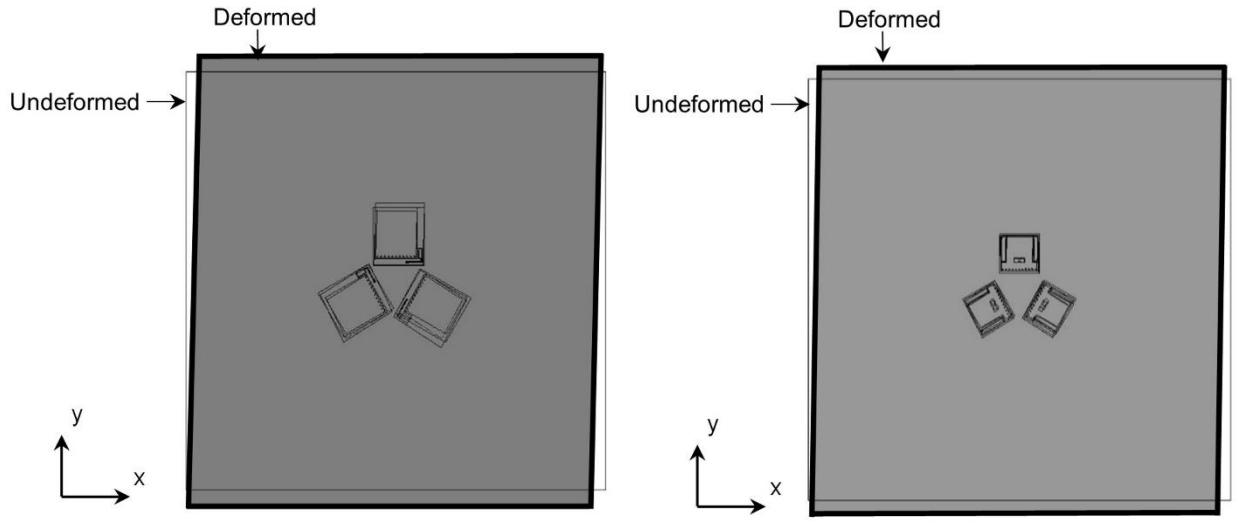

(a) Rosette with folded patch antenna sensors (b) Rosette with slotted patch antenna sensors

Figure 9. Aluminum plate applied with surface strain field with $\epsilon_x = -400$ με, $\epsilon_y = 600$ με, and $\epsilon_{xy} = 200$ με

Table 6. Comparison of calculated strain components (Unit: με)

Strain	Strain applied in the aluminum plate	Folded patch antenna sensor		Slotted patch antenna sensor			
		Calculated strain		Transverse strain effect considered		Transverse strain effect not considered	
		Strain	Error	Strain	Error	Strain	Error
ϵ_x	-400	-409.336	2.33%	-403.787	0.95%	-232.130	41.97%
ϵ_y	600	606.410	1.07%	601.532	0.26%	486.305	18.95%
ϵ_{xy}	200	191.583	4.21%	208.491	4.25%	148.994	25.50%

5 Summary

In this paper, strain rosettes with folded patch antenna sensors and slotted patch antenna sensors are presented. The strain sensing performance is validated by mechanics-electromagnetics coupled simulation using ANSYS. The transverse strain effect of both sensors has been discussed and validated through laboratory experiments. Numerical analysis shows the linear relationship between the resonance frequency of the antenna and the strain. Compared with slotted patch antenna, folded patch antenna does not have transverse strain sensitivity and this property makes its application more straightforward. The numerical simulation demonstrates that strain components obtained by both rosettes are close to those applied on the aluminum plate, which validates the potential of both rosettes for measuring an arbitrary surface strain field. Future work will focus on the fabrication of the strain rosette and strain sensing testing through laboratory experiments.

Acknowledgement

This material is based upon work sponsored by the INSPIRE University Transportation Center through USDOT/OST-R grant #69A3551747126. The first author is partially supported by Chinese Scholarship Council (#201406260201). Any opinions, findings, and conclusions or recommendations expressed in this publication are those of the authors and do not necessarily reflect the view of the sponsors.

References

Boresi, A. P. & Schmidt, R. J. 2002. *Advanced Mechanics of Materials*, John Wiley & Sons, Inc.

Butler, J. C., Vigliotti, A. J., Verdi, F. W. & Walsh, S. M. 2002. Wireless, passive, resonant-circuit, inductively coupled, inductive strain sensor. *Sensors and Actuators A: Physical,* 102**,** 61-66.

Carver, K. R. & Mink, J. M. 1981. Microstrip antenna technology. *IEEE transactions on antennas and propagation,* 29**,** 2-24.

Cho, C., Yi, X., Li, D., Wang, Y. & Tentzeris, M. M. to be published. Eigenvalue perturbation solution for the Multi-physics simulation of antenna strain sensors. *IEEE journal on Multiscale and Multiphysics Computational Techniques*.

Daliri, A., Galehdar, A., John, S., Wang, C. H., Towe, W. S. T. & Ghorbani, K. 2012. Wireless strain measurement using circular microstrip patch antennas. *Sensors and Actuators A: Physical,* 184**,** 86-92.

Daly, P. 1971. Hybrid-mode analysis of microstrip by finite-element methods. *IEEE Transactions on Microwave Theory and Techniques,* 19**,** 19-25.

Deshmukh, S. & Huang, H. 2010. Wireless interrogation of passive antenna sensors. *Measurement Science and Technology,* 21**,** 035201.

Epcglobal Inc. 2008. EPC™ Radio-frequency Identity Protocols Class-1 Generation-2 UHF RFID Protocol for Communications at 860 MHz-960 MHz EPCglobal Inc.

Jin, J.-M. & Volakis, J. L. 1991. A hybrid finite element method for scattering and radiation by microstrip patch antennas and arrays residing in a cavity. *Antennas and Propagation, IEEE Transactions on,* 39**,** 1598 - 1604.

Merilampi, S., Björninen, T., Ukkonen, L., Ruuskanen, P. & Sydänheimo, L. 2011. Embedded wireless strain sensors based on printed RFID tag. *Sensor Review,* 31**,** 32-40.

Occhiuzzi, C., Paggi, C. & Marrocco, G. 2011. Passive RFID Strain-Sensor Based on Meander-Line Antennas. *Antennas and Propagation, IEEE Transactions on,* 59**,** 4836 - 4840.

Spencer, B. F., Jr., Ruiz-Sandoval, M. E. & Kurata, N. 2004. Smart sensing technology: opportunities and challenges. *Structural Control and Health Monitoring,* 11**,** 349-368.

Tan, E. L., Pereles, B. D., Shao, R., Ong, J. & Ong, K. G. 2008. A wireless, passive strain sensor based on the harmonic response of magnetically soft materials. *Smart Materials and Structures,* 17**,** 025015.

Tata, U., Huang, H., Carter, R. L. & Chiao, J. C. 2009. Exploiting a patch antenna for strain measurements. *Measurement Science and Technology,* 20**,** 015201.

Yi, X., Cho, C., Cook, B., Wang, Y., Tentzeris, M. M. & Leon, R. T. 2013a. Design and simulation of a slotted patch antenna sensor for wireless strain sensing. *Proceedings of SPIE, Nondestructive Characterization for Composite Materials, Aerospace Engineering, Civil Infrastructure, and Homeland Security.* San Diego, California, USA.

Yi, X., Cho, C., Cook, B., Wang, Y., Tentzeris, M. M. & Leon, R. T. A slotted patch antenna for wireless strain sensing. Proceedings of the ASCE 2014 Structures Congress, April 3-5 2014 Boston, MA, USA.

Yi, X., Wang, Y., Tentzeris, M. M. & Leon, R. T. 2013b. Multi-physics modeling and simulation of a slotted patch antenna for wireless strain sensing. *Proceedings of the 9th International Workshop on Structural Health Monitoring (IWSHM).* Stanford, CA, USA.

Yi, X., Wu, T., Wang, Y., Leon, R. T., Tentzeris, M. M. & Lantz, G. 2011. Passive wireless smart-skin sensor using RFID-based folded patch antennas. *International Journal of Smart and Nano Materials,* 2**,** 22-38.

Figure captions

Table captions